


Disorder-induced enhancement of entanglement growth in one dimension: Information leakage at the scale of the localization length

Roopayan Ghosh and Arnab Das

School of Physical Sciences, Indian Association for the Cultivation of Science, Jadavpur, Kolkata 700032, India

 (Received 3 March 2020; revised 13 November 2020; accepted 19 December 2020; published 12 January 2021)

When a group of compactly packed free fermions is allowed to spread over an empty one-dimensional lattice, the spreading particles can create entanglement between different parts of the lattice. We show, although breaking of translational invariance (TI) of the lattice by disorder slows down the spreading of local observables, the entanglement entropy of a subsystem can nonetheless receive a remarkable enhancement as long as the subsystem lies within the single-particle localization length. We show the main mechanism behind this enhancement is the reentrant exchange of particles between the subparts due to transport of mutual information due to backscattering. We discuss the length and timescales relevant to the phenomenon. We study the phenomenon for breaking of TI by both quasiperiodic and random potentials. We further explore the effect of randomness only in the initial state. This also exhibits a similar enhancement effect even in a TI lattice. We also touch upon the special case of periodic potential where qualitatively similar phenomenology emerges, although the coherence in the backscattering in this case leads to effects not captured by our simple yet generic picture.

DOI: [10.1103/PhysRevB.103.024202](https://doi.org/10.1103/PhysRevB.103.024202)

I. INTRODUCTION

In this paper we study the effect of disorder on the dynamics of entanglement formation between two nonoverlapping parts of a one-dimensional lattice due to spreading of noninteracting fermions on the lattice over time.

Dynamics of spreading of particles and entanglement in such setups have widely been studied under the general protocol “inhomogeneous quench” for translationally invariant (TI) lattices [1–11] as well as in some special systems where translational invariance is broken locally (local quenches) [12–15] or in critical systems where conformal symmetry dictates the dynamics [16–30]. Here we study the effect of extensive (i.e., spread over the entire lattice) disorder in the form of random and quasiperiodic potentials on the growth of entanglement in the absence of any simplifying symmetry.

A suitable initial state for studying such spreading dynamics is the so-called “domain-wall state” where one part of the lattice is completely filled whereas the rest of the lattice is empty (domain wall refers to the boundary between the completely filled and the completely empty parts). This initial state has been used for most of the above-mentioned works as well as for illustrating most of our results here.

Already in the TI case, the dynamics of the entanglement entropy (EE) of a subsystem of the lattice exhibits a curious feature if one starts with a domain-wall-like initial state: Whereas the spreading of the particle density is linear in time, the entanglement entropy of the subsystem grows logarithmically with time [1,31]. Such slow growth of entanglement is a hallmark of many-body localization [32–35] where the disorder suppresses the growth of entanglement. In this case, however, the slow entropy growth happens in the presence of total translational invariance.

What we show here is, introduction of disorder actually has an *opposite effect* in this case—it actually *enhances* the entanglement growth substantially as long as the subsystem in question is within the localization length from the initial domain wall. We also show that within the relevant length scale, the entanglement growth is linear in time. The most spectacular manifestation of the phenomenon is in the weak disorder limit when the localization length is large.

For disordered (quasiperiodic or random) systems, we identify incoherent backscattering as the main mechanisms behind this enhancement in the entanglement entropy. We also study the effect of the strength of the TI-breaking potential in spreading of the entanglement. Since for weak disorder the localization length is significantly large, the understanding of the phenomenon might play a role in designing systems for efficient storage and transfer of information in the presence of disorder in quantum devices.

Finally, we explore the effect of randomness put solely in the initial state and demonstrate that the well-known result of logarithmic growth of entanglement in the TI case for a single domain-wall initial state [1–3,36] is a rather fine-tuned result—small disorder in the occupied domain can turn this logarithmic growth to a linear one. Our paper also shows the phenomenon of enhancement of entanglement due to breaking of TI of the lattice is not fine-tuned and is robust to random variation of initial states within a certain form.

We also provide a glimpse of the phenomenology in a rather special case of TI breaking, namely, the one due to periodic potentials where a qualitatively similar enhancement of entanglement is observed. However, coherence in scattering due to the regularity of the lattice structure also plays a dominant role, making the scenario more complex. We find entanglement entropy growth shows a $a \ln t + b$ scaling

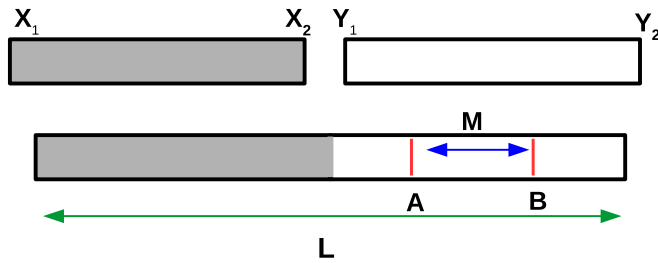


FIG. 1. A schematic showing the case of inhomogeneous quench. In an inhomogeneous quench we take two systems X_1X_2 and Y_1Y_2 and glue X_2 and Y_1 together at $t = 0$. The system X_1X_2 has a different filling fraction (denoted by the gray shade) than Y_1Y_2 . AB denotes the subsystem considered in the paper. The system size is denoted as L , and the subsystem size is denoted as M , which represents the number of sites. See the text for details.

behavior for the lattice periodicity $p \ll L$ with the coefficient $a \propto p$. We also recover the linear scaling behavior found in the TI case [15] for $p \sim L/2$. We then discuss the respective regimes of periodicity where one expects the two different behaviors. Curiously, although the backscattering is still the dominant mechanism of enhancement of entanglement even in the periodic case, we do not see greater enhancement with an increased number of scatterer/unit length here, rather, the above scaling relations imply a higher growth rate with larger p , i.e., a smaller number of scatterers per unit length. Coherence in the scattering from the periodically placed scatterers forbids simple addition of contributions from different scatterers (a detailed analysis of this is outside the remit of this paper).

The plan of the rest of the paper is as follows. In Sec. II we discuss the model Hamiltonians and give a brief summary of the various cases we consider and quantities we calculate. Then in Sec. III we discuss in detail the cases of a random disordered potential and a quasiperiodic (Fibonacci) potential, showing the growth of entanglement entropy in various scenarios, discuss the scalings, and explore various factors that control the spreading. Then in Sec. IV we touch upon the behavior of periodic lattices, and finally in Sec. V we discuss our observed results and conclude.

II. THE SETUP

Figure 1 describes our quench in a schematic. We take one system X_1X_2 with a certain particle density and another system Y_1Y_2 with a different particle density and then at $t = 0$ glue X_2 and Y_1 together and let the system evolve. This difference in particle densities will induce a flow of particle current which, in turn, creates entanglement between the two halves of the system. Equivalently, we can consider the full system X_1Y_2 and start with a domain-wall initial state with a domain wall at $i = L/2$ separating the different density sectors. This picture may be more useful for qubit systems for specific initial states where using Jordan-Wigner transformation, one can go from the spin-1/2 language to the fermionic language and would end up with a domain-wall initial state with densities 0 and 1 on two sides. Additionally, the domain-wall picture is easier to use for analysis, and we will refer to it in rest of our paper.

Throughout the paper, the model Hamiltonian used for calculations is

$$\mathcal{H} = -\frac{J}{2} \sum_m (c_m^\dagger c_{m+1} + c_{m+1}^\dagger c_m) + J \sum_m \mu_m c_m^\dagger c_m, \quad (1)$$

where c_m [c_m^\dagger] are fermion annihilation [creation] operators and μ_m is the form of the on-site potential which we will take to be random, quasiperiodic, or periodic. The Hamiltonian is now scaled in units of J which is the hopping strength. The specifics of the setups are as follows.

(1) *Quasiperiodic*. We will consider the quasiperiodic potentials which can be viewed as a superposition of multiple periodic potentials with incommensurate periods. We will focus on an example of such a sequence, namely, the Fibonacci word sequence in the main text. A Fibonacci sequence is generated by the following recursion relation:

$$F_n = F_{n-1} + F_{n-2},$$

with $F_0 = 0$ and $F_1 = 1$. Thus, the well-known Fibonacci sequence looks like 0, 1, 1, 2, 3, 4, 8, 13, Later, Chuan [37,38] introduced a concept of Fibonacci words, defined on the alphabet set $\{0, 1\}$ in which the length of the n th word in the sequence is given by F_n . These words are generated by the concatenation of the previous two words. Formally, $S_n = S_{n-1}S_{n-2}$ where S_n is the n th Fibonacci word. S_0 is taken to be 0 and $S_1 = 01$. Thus, the first few terms of the words are as follows:

$$\begin{aligned} S_0 &= 0, & S_1 &= 01, & S_2 &= 010, & S_3 &= 01001, \\ S_4 &= 01001010, \\ &\vdots \end{aligned}$$

Even at $N \rightarrow \infty$ it can be shown that S_N has no periodicity, and the word is unique. However, it is clear that the letters (digits) in the word are correlated.

For a system of size L , where L is chosen to be a number in the Fibonacci sequence, we generate the Fibonacci word sequence and then define

$$\begin{aligned} \mu_i &= \mu_0 - \delta\mu, & S_L^i &= 0 \\ \mu_i &= \mu_0 + \delta\mu, & S_L^i &= 1, \end{aligned} \quad (2)$$

where we have labeled the i th letter (digit) in S_n as S_n^i . This can be shown to result in a quasiperiodic lattice [39–43].

(2) *Random*. The potential on-site μ_m is chosen randomly between $\mu - \delta\mu$ and $\mu + \delta\mu$. For numerical calculations averaging over several realizations of the random numbers is performed.

(3) *Periodic*. We choose to work with two kinds of periodic potential.

(a) $\mu_m = \mu_0 + (-1)^{\sum_{n=1}^L \delta_{m,np}} \delta\mu$. This represents a periodically varying potential with period p in which every p th site has a potential $\mu - \delta\mu$ and every other site has a potential $\mu + \delta\mu$.

(b)

$$\begin{aligned} \mu_m &= \mu_0 + \delta\mu, & m &= 1 \cdots q/2, \\ \mu_m &= \mu_0 - \delta\mu, & m &= q/2 + 1 \cdots q \end{aligned}$$

repeated over all the length of the lattice, i.e., a square pulse potential varying between $\mu_0 + \delta\mu$ and $\mu - \delta\mu$ with period q .

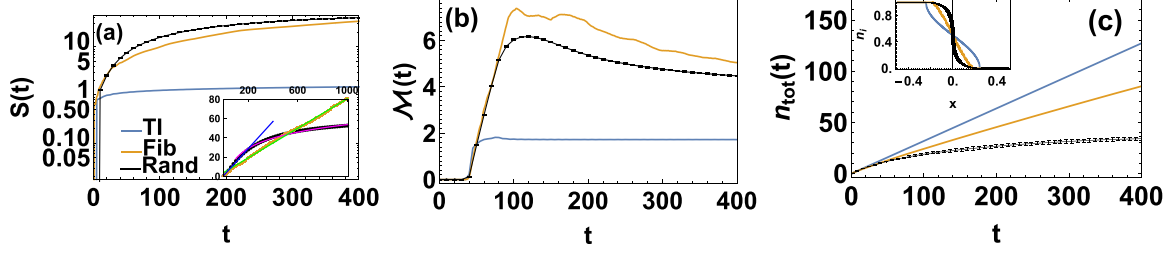


FIG. 2. Growth of entanglement entropy, mutual information, and local densities and correlations for various lattices. We have taken $L = 2048$ for the TI and the random case and $L = 2584$ for the Fibonacci case. (a) Plot of the entanglement entropy S vs time (in units of J^{-1}) for a subsystem of size $M = L/2$. The site A (see Fig. 1) is chosen at $i = L/2 + 1$, $\mu = \delta\mu = 0.1$. We have averaged over 2000 disorder realization for the random potential cases. The enhancement of entanglement due to the breaking of translational invariance is clearly visible. This is quite in contrast with the spreading of the density of the particles, which is seen to have a slower spreading in TI-broken systems as expected [shown in (c)]. The inset shows the fit of entanglement entropy vs t for the disordered cases. The blue line denotes linear fit to $0.747 + 0.14t$ whereas the magenta line denotes a logarithmic fit to $-50.43 + 15.03 \ln t$ in the two time regimes where the particles move within and beyond the localization length of the system. The green line is the fit for entanglement entropy growth for Fibonacci systems, which is linear and is $3.97 + 0.07t$ (b). Plot of mutual information vs time for subsystem α spanning sites $i = L/2 + 1$ to $i = L/2 + 40$ and β -spanning sites $i = L/2 + 41$ to $i = L/2 + 80$. (c) This frame shows the growth of total density within the initially empty subsystem with time: $n_{tot} = \sum_{i=L/2+1}^L \langle c_i^\dagger c_i \rangle$ vs t . The inset is showing $n_i = \langle c_i^\dagger c_i \rangle$ at time $t = 500$ vs the normalized lattice coordinate x [$x = (i - L/2)/L$], giving us the idea of spreading/localization in space until the given time.

These two sequences yield qualitatively similar results as will be shown in Sec. IV.

We consider a system with L sites with open boundary conditions occupied by $L/2$ spinless fermions with the initial condition,

$$\begin{aligned} \langle c_m^\dagger c_n \rangle &= \delta_{mn}, \quad m \leq L/2, \\ &= 0, \quad \text{otherwise.} \end{aligned} \quad (3)$$

Starting from $t = 0$, our aim is to study the evolution of entanglement between the subsystem AB and the rest of the environment. We would calculate two quantities, Von Neumann entropy and mutual information for this purpose.

To calculate Von Neumann entropy, we first choose a subsystem of M sites. For most cases we would deal with a subsystem of $i = L/2 + 1$ to $i = L/2 + M$ which gives the same S value as a subsystem chosen between $i = L/2$ and $i = L/2 - M + 1$. We will mostly focus on the case when $M = L/2$, i.e., the bipartite system.

Since our Hamiltonian is bilinear in fermions, all its many-body eigenfunctions can be written as Slater determinants of one-body eigenfunctions. Hence, one can write the Von Neumann entropy for any instant of time t as [44,45]

$$S(t) = \sum_{i=1}^M \lambda_i(t) \ln \lambda_i(t) + [1 - \lambda_i(t)] \ln [1 - \lambda_i(t)], \quad (4)$$

where $\lambda(t)$'s are the eigenvalues of $C_{mn}^{\text{res}}(t)$. $C_{mn}(t) = \langle c_m^\dagger(t) c_n(t) \rangle$, and *res* denotes indices restricted to the subsystem under consideration.

$\langle c_m^\dagger(t) c_n(t) \rangle$ can be exactly calculated for any value of time using the Heisenberg picture. For our system the expression can be written in terms of single-particle eigenfunctions and eigenvalues as

$$\langle c_m^\dagger(t) c_n(t) \rangle = \sum_{k,l,i,j} R_{km} R_{ln} R_{ki} R_{lj} e^{i(E_k t - E_l t)} \langle c_i^\dagger(0) c_j(0) \rangle, \quad (5)$$

where E_k 's are the one-particle eigenvectors and R is the unitary matrix diagonalizing the one-particle sector of the

Hamiltonian (See Appendix for details). We also measure the mutual information between two subsystems labeled by α and β is defined as follows:

$$\mathcal{M}^{\alpha\beta} = S^\alpha + S^\beta - S^{\alpha \cup \beta}. \quad (6)$$

III. THE DISORDERED CASE

A. Enhancement of entanglement

The central result is summarized in Fig. 2. It shows the growth of half-chain entanglement entropy S of the lattice, starting from a domain-wall-like initial state where half of the system is full, and the rest is empty. The comparison has been made between lattices with TI, quasiperiodic Fibonacci, and a random disordered potential, respectively.

The left frame [Fig. 2(a)] shows that whereas the growth of half-chain entanglement is extremely slow for the TI case, and a remarkable enhancement in the growth occurs when the TI is broken by introduction of disorder via the Fibonacci and random potentials, respectively. The middle frame shows similar enhancement of growth dynamics for the mutual information $\mathcal{M}(t)$ due to disorder.

The middle frame compares between growth of mutual information for two adjacent subsystems α -spanning sites $i = L/2 + 1$ to $i = L/2 + 40$ and β -spanning sites $i = L/2 + 41$ to $i = L/2 + 80$ in a TI lattice, a Fibonacci lattice, and a random lattice, respectively. For both cases of disorder, the growth of mutual information is much higher compared to the TI case.

In contrast, the right frame [Fig. 2(c)] shows the particle density in the initially empty subsystem grows much faster in the TI case compared to the two disordered cases as expected. The inset of Fig. 2(c) shows the spatial distribution of the particle at $t = 500$. Until this time, the spreading in the TI case is appreciably larger compared to the disordered cases. The inset of Fig. 2(a) shows the growth of entanglement entropy in the random and Fibonacci potential cases, respectively. It clearly shows two qualitatively different behaviors for two

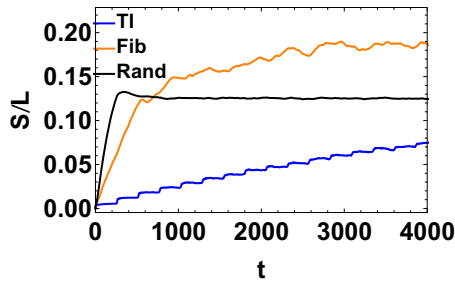


FIG. 3. The figure illustrates the mechanism of increase in entanglement entropy S of the subsystem of size $M = L/2$ for a system of length $L = 256$. Averaging has been performed over 80 disorder realizations. In the TI case, the slow (logarithmic) growth is boosted by a steep jump periodically in time with roughly a time period ~ 256 . This is approximately the time taken by a particle to exit the subsystem and reenter it after getting reflected from the (open) boundary of the system as particle propagation is ballistic in TI systems [1,49]. This illustrates that the faster growth of S on top of the logarithmic one is due to reentrance of the particles to the subsystem after getting backscattered (in the TI case from the boundary). For the disordered (quasiperiodic/random) cases, there are random scatterers throughout the entire lattice, and, hence, the enhancement of S is extensive, and the steps are smeared out. This results in a superlogarithmic (linear) growth of S .

different timescales for the random disordered case. When the propagating wave front is within the maximum Thouless localization length [46] (~ 250 for the system considered), the entropy increases linearly, but once the wave front goes beyond that, further particle movement gets exponentially suppressed, and the growth of EE gets suppressed logarithmically before reaching a steady value. The linear increase can also be gleaned from Fig. 3. For a quasiperiodic Fibonacci system since there is no localization in the wave function, the linear regime continues for a much longer time before reaching the steady-state value based on system size. The linear regime is presented in the inset. This is in contrast to the behavior expected in the interacting integrable and nonintegrable systems where one expects a power-law t^β , $\beta < 1$ rise in entanglement entropy for short timescales for the propagating domain wall before a linear regime arrives at large timescales and finally saturates [17,47,48].

B. The mechanism

Entanglement between a system and its environment is generated not only when a particle enters into the environment from the system, but also when a particle returns/bounces back from the environment to the system. The mechanism manifests itself most clearly in spreading of particles on a finite TI system with reflecting boundaries. Let us consider a TI lattice, a part of which (consecutive lattice sites) entirely filled (system) with particles and the rest completely empty (environment). Now for a quench with such domain-wall-like initial states as is already known, the entanglement between the system and the environment (measured by the entanglement entropy S of any of them) grows logarithmically with time. However, if the system is finite, then the particles after exiting the system traverse the environment, get reflected from the lattice boundary, and reenter the system. This produces

initial jumps in S at regular time intervals proportional to the average time taken by the particle to leave the system and reenter. Figure 3 precisely shows this. Here we consider a setup where the initial state is a half-filled domain-wall state. We refer to the initially filled half of the lattice of size L as the system and the initially empty half as the environment. The first hike in S is close to $t = 0$ due to the entry of the particles to the environment right at the onset of the dynamics. The next step/jump (the first visible one in Fig. 3) appears around $t \sim L = 256$, which is roughly the time elapsed between the exiting of a particle from the system and reentering it after getting reflected from the lattice boundary once after traversing the environment. The subsequent early jumps appear around $t = nL$ where n is an integer. But with the melting of the domain wall, the interval between the jump changes, and since the system is finite, the steps flatten out eventually approaching the saturation.

When TI is broken extensively by disorder, then particles scatter back incoherently to the system from all parts of the environment, and that results in a steady increase in S —the steps due to contribution from different scatters superimposes, resulting in a smooth power-law (approximately linear as discussed in the previous section) growth of S as shown in Fig. 3. It is worth noting that the breaking of TI does not produce a net enhancement in the EE in cases of the local or global quenches in system with relatively sparse and uniform particle distribution [50–53]. Although there is a contribution of backscattering due to the breaking of TI leading to an enhancement in the EE also in those cases, it does not supersede the cut in the EE growth produced by the effect of localization there. This is because in those cases the growth of EE relies mainly on the transport of extensive number of particles/quasiparticles from all over the system, and localization limits that in a severe manner. This extensive cut cannot be compensated by the enhancement due to the backscattering, which is proportional to the area of the domain boundary in the localized case (only comes from the states within a localization length around the domain boundary).

C. The relevant length and timescales

Clearly, the intriguing feature here is the dynamics of entanglement within a length scale (subsystem size) comparable to the localization length. Needless to say, far beyond the localization length, there will be practically no spreading of particles due to localization in the disordered cases, and, hence, the entanglement growth will saturate to a value which is proportional to the localization length. Figure 6 shows the different saturation values corresponding to different localization length. For a low to intermediate disorder strength where the localization length is large but smaller compared to the length of the system, we see a power-law fit $S^{\text{sat}} \sim \frac{1}{\delta\mu^{1.82}}$, which clearly indicates the rapid rise in saturation entanglement entropy with larger localization lengths. In contrast, in the TI case, the particles will eventually spread everywhere, hence, despite the logarithmically slow growth of entanglement in this case, the half-chain entanglement for the TI case will overtake the values for the disordered cases after a sufficiently long time. However, this timescale in which the TI value will match the saturation value of the disordered case

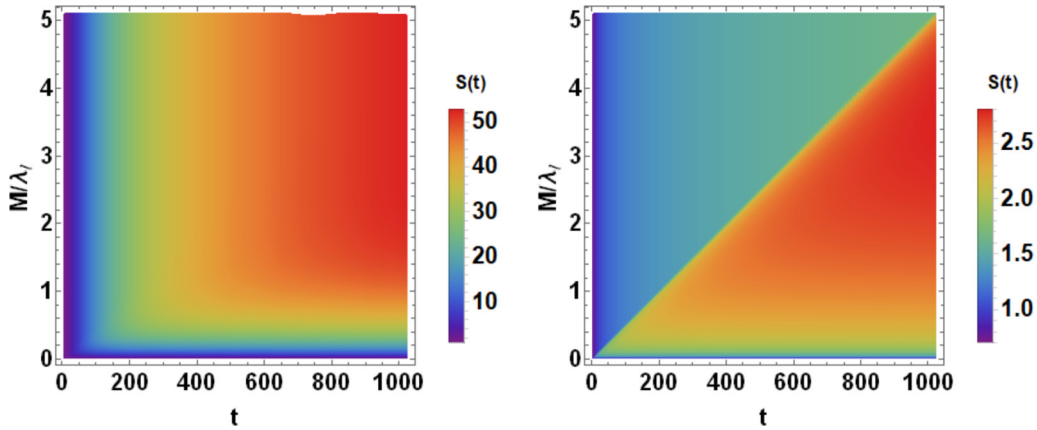


FIG. 4. Spatiotemporal scale of the enhancement phenomenon. Left panel: Half-chain entanglement entropy $[S(t)]$ as a function of subsystem size (M) (scaled by the maximum Thouless localization length of the system λ_l) and time (t) for a disordered system of size $L = 2048$ and $\mu = \delta\mu = 0.1$. Averaging has been performed over 80 disorder realizations. Right: Same as the left panel but for a translationally invariant system.

can be enormously large especially for a weakly disordered system since the growth is logarithmically slow in the TI case.

The relevant timescales and length scales can be studied by taking the subsystem to be of length M and putting one end of it at the domain-wall boundary and studying the growth of the entanglement entropy S of the subsystem as function of the evolution time t and subsystem size M as shown in Fig. 4. The left panel of Fig. 4 shows the value of subsystem entanglement entropy S as a function of the evolution time t and the subsystem size M (scaled by the Thouless localization length λ_l). The right frame shows the TI case.

From the left frame we see for a given M the entanglement S saturates rapidly with time. The saturation time naturally increases with M (roughly linearly). As M continues to increase, the saturation time eventually becomes independent of M , i.e., saturates as a function of M , close to $M \sim \lambda_l$. This is because it is actually the underlying localization length that dictates the final extent of spreading. To visualize this clearly, we fix t to a sufficiently large value (so that saturation is reached for all M 's), and M is increased. Then the value to which S saturates increases with M meaning the saturation value of S scales with M (volume law). However, as M crosses the localization length λ_l ($M/\lambda_l \approx 1$), then the saturation value of S (as a function of M) stops increasing any further and settles to a maximum value. This is because the spreading of the particles beyond the localization length is negligible, hence, increasing the subsystem beyond that does not contribute to further enhancement of the saturation value of S . The right panel shows the TI case. Here there is, of course, no typical length scale beyond which the saturation time for a fixed M is independent of M —it is always proportional to M (albeit logarithmically [50,54–60]) as can be seen clearly from right panel of Fig. 4. The linear contour for saturation of S is formed diagonally. This is expected since in a TI system the entanglement grows until the particles spread over the whole of M (there is no smaller cutoff, e.g., due to the localization). The enhancement of the spreading of S in the disordered case compared to the TI case is limited to within the length scale of order λ_l . Beyond that scale, the growth in the TI case continues, whereas the disordered case comes to a saturation.

D. Tuning the disorder strength

The enhancement is most prominent for an intermediate disorder strength. The disorder has two competing effects—on one hand, it enhances the backscattering rate which aids the growth of S , on the other hand, it strengthens localization which arrests the spreading of the particles and suppresses the growth. This results in a nonmonotonic behavior of $S(t^*)$ measured after a given evolution time t^* as a function of the strength $\delta\mu$ of the disordered part of the potential in the respective Hamiltonians for the Fibonacci and random cases. Initially, S^* increases with $\delta\mu$ compared to the value of S^* for the TI case due to enhanced backscatterings and reaches a peak. Then, with a further increase in $\delta\mu$ it reduces sharply and falls below the TI value. This is demonstrated in Fig. 5. Here we consider an initial domain-wall state of width $L/2$ for a lattice of system-size $L = 2048$ and a subsystem AB of length $M = L/2 - 20$ with its end A at $i = L/2 + 21$, i.e., 21 lattice sites away from the domain-wall boundary (see Fig. 1). The entanglement entropy S of AB is measured. (See also Appendix C). The competing effect of the disorder strength is reflected in the nonmonotonic behavior of $S(t = 500)$ as a function of $\delta\mu$. Dynamics for different values of $\delta\mu$ are also shown in Figs. 5(b) and 5(c). Whereas for $\delta\mu = 0.1$, the disorder clearly results in a pronounced enhancement compared to the TI case (although the random disorder shows a faster saturation at late times), and for $\delta\mu = 5.0$, the growth is suppressed below that in the TI case even at small timescales. This competing effect is also visible in Fig. 2(b) where the mutual information between the two subsystems in the random disordered case shows a lower value than the Fibonacci potential due to the onset of localization. At extremely late times, however, when the entropy saturates, the strength of localization is the only factor determining the saturation value of entropy, as evident from Fig. 6.

E. Randomness in the initial state

We have also studied the effect of randomness put solely in the initial state keeping the TI of the lattice intact. To this end we construct the r.d.w. as follows. Let r be a pseudorandom

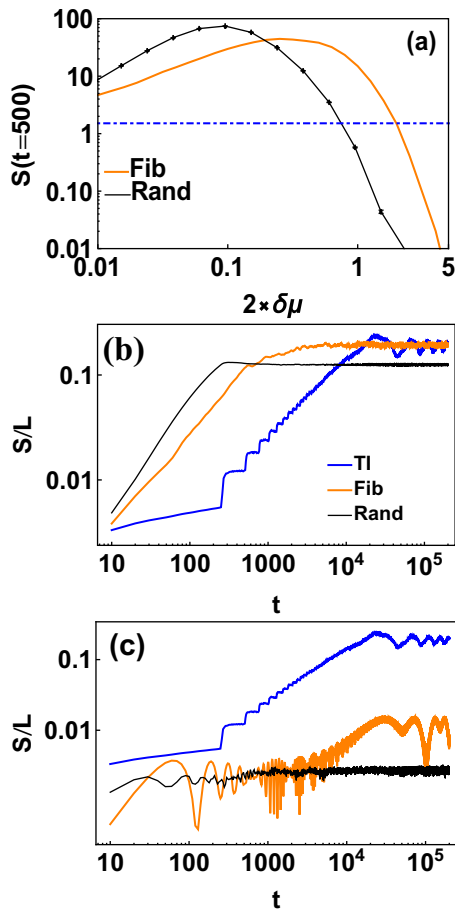


FIG. 5. The figure demonstrates the competing effects produced by the disorder on enhancement of the entanglement growth of a subsystem of one-dimensional lattices (see the text for the details of the geometry), compared to the TI case of same geometry. Frame (a) shows the consequent nonmonotonic behavior of the entanglement $S(t = t^*)$ as a function of the disorder strength μ for a system size $L = 2048$. Here we have taken $t^* = 500$. The horizontal dashed-dot (blue) line marks the value of $S(t = 500)$ for the TI case. Frames (b) and (c) show the dynamics of S for $\mu = \delta\mu = 0.1$ and $\mu = \delta\mu = 5.0$, respectively. We have taken $L = 377$ for the Fibonacci lattice and $L = 256$ for the random case.

number between 0 and 1, then the initial state is chosen such that $\langle c_i^\dagger c_j \rangle = \delta_{ij}$ for $i < L/2$, $r > \mathcal{P}$, and 0 otherwise. \mathcal{P} , thus, defines the probability a site is occupied in the left half of the system. The right half is kept completely empty. We only use one representative initial state for each probability value to show the scenario, and for the disordered Hamiltonian we average over 80 disorder realizations. Our result shows that the logarithmically slow growth of entanglement in the TI case with a single domain-wall (d.w.) initial state [1–3,36] is a fine-tuned result. We find, the small randomness present in a r.d.w. initial state is enough to make the growth behavior switch from logarithmic to a linear time dependence in a TI lattice (see Fig. 7).

The figure also shows, a further enhancement of entanglement growth (over the TI case with the r.d.w.) can be achieved in a quantitative level if disorder is added to the lattice. This increase, however, is visible for $\mathcal{P} > \mathcal{P}_c$, dependent of the

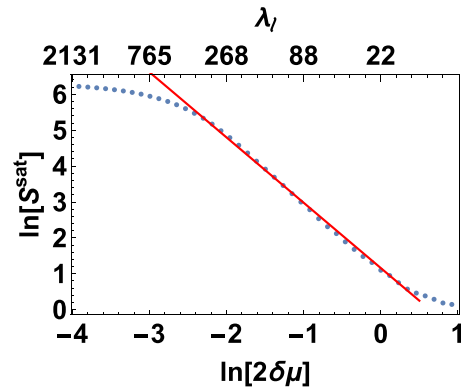


FIG. 6. Plot of $\delta\mu$ vs S^{sat} which denotes the saturation value of the half-chain entanglement entropy after time $t \sim 10^{10}$ for $L = 4096$. The x axis is also labeled by the maximum Thouless localization length λ_l corresponding to $\delta\mu$. The red line denotes the fit to $1.16 - 1.82 \ln(2\delta\mu)$.

type of disorder as is evident from the inset of the plot. This is expected as both being similar effects, the effect due to disorder in initial state must be low for the effect due to disorder in the potential to be seen. In this sense, the phenomenon of enhancement of entanglement due to breaking of lattice TI is not fine-tuned to a particular initial state and is quite robust to the random variation over the r.d.w. initial states we have considered.

IV. THE PERIODIC POTENTIAL CASE

In this section we will skim over the scenario where we break the translational invariance of the system by introducing a spatially periodic potential. Clearly such a system still possesses a translational symmetry of the Z_n class and, thus, is different from the systems in the previous section which had

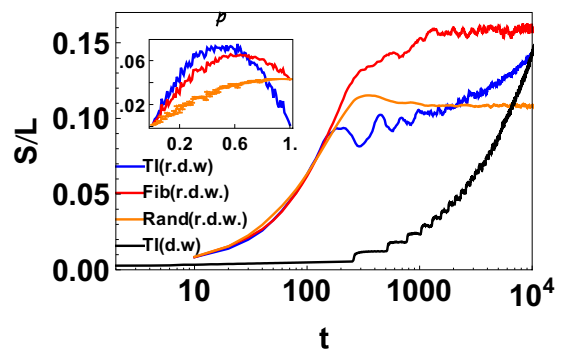


FIG. 7. The figure compares growth of entanglement S with time for the r.d.w. initial state (for $\mathcal{P} = 0.6$) on a TI lattice with those for the d.w. state in a TI lattice, r.d.w. states on a Fibonacci lattice, and a random lattice, respectively. The result shows that the small randomness even just in the initial state (the r.d.w. case) is sufficient to switch the logarithmic entanglement growth observed in the TI lattice case with the d.w. initial state to a linear growth (see growth until $t \sim 200$) generic to the TI broken lattice cases (also shown for comparison). Results are for ($L = 256$, $\delta\mu = 0.2$). The inset shows behavior of S at $t = 500$ for $L = 1024$ as a function of \mathcal{P} (see the text for details) for a r.d.w. state.

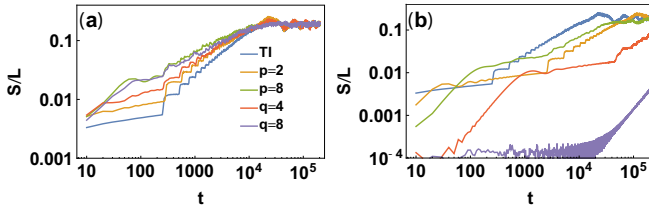


FIG. 8. Plot of a comparison of half-chain entanglement entropy growth of a system of length $L = 256$ for the TI system and periodic systems of both kinds with periodicity $p = 2, 8$ and $q = 4, 8$ for (a) $\mu = \delta\mu = 0.1$ and (b) $\mu = \delta\mu = 5$, showing the increase in entanglement entropy with higher periodicity for both p and q types of periodicity for lower strength of potentials and showing the difference between them for a large potential strength. Note that $p = 2$ and $q = 2$ defines the same potential.

no such symmetry. Figure 8 shows results for the dynamics of the system when a periodic potential is applied for the same parameter values as Figs. 5(b) and 5(c). Here we clearly see that for low $\delta\mu$, the entanglement entropy value increases with increasing periodicity p and q . This is a counterintuitive result in the first glance since one would expect a higher number of scattering centers present for lower values of p and q . However, due to the periodicity of the lattice the scattered wave fronts interfere coherently unlike in the previous section which results in a counterintuitive scenario. For a concrete understanding, one requires a thorough analytical analysis of this phenomenon, which is involved and left for a future work. In this present paper, we focus on the various interesting features which occur in this setup.

As can be seen from Fig. 8(b) for large values of $\delta\mu$ entanglement entropy for the q -type periodic potential is heavily suppressed and $q = 8$ shows lower entanglement than $q = 4$ contrary to the case with p and the results of Fig. 8(a). This is simply due to the fact that the q -type potential suppresses particle tunneling more than the p -type potential due to its nature of being a series of square barrier potentials than the δ function one (shown in the inset of Fig. 9). Additionally, the suppression is larger for larger q because the width of the barrier increases with increasing q . Since, at high potential strength particle diffusion plays the most important role in determining entanglement entropy, this factor heavily reduces entanglement growth, and we get the current result.

In the rest of this section we would take $\mu = \delta\mu = 0.1$ unless otherwise specified. Figure 9 shows the fit of $S(t)$ for $t < L$ for periodic potentials of different kinds and periodicities for a low potential strength $\mu = \delta\mu = 0.1$. It is seen that the growth in S_{vN} follows $a + b \ln(t)$ behavior if $t \sim L$ is sufficiently large for periodic potential systems. This is reminiscent of a similar behavior seen in conformally invariant TI systems under local/geometric quench [1,50]. However, since once we break TI the system is gapped and no longer expected to be conformally invariant, so we do not, in general, expect this to hold. It can be seen after oscillatory behavior at initial times the fit is quite good. The plot of fit coefficient b vs p is provided in Fig. 11(a) as well. It is a straight line with a slope close to 0.167. For TI systems, it is known that the entanglement growth for inhomogeneous quenches [1] can be fit at time $t < L$ for large L to $c/6 \ln t$ where c the central

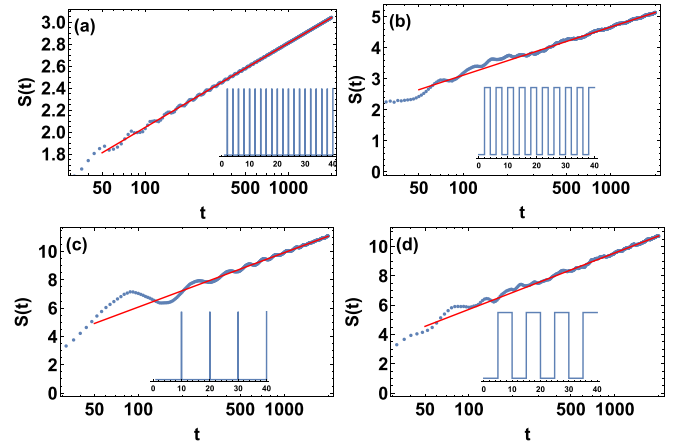


FIG. 9. (a) Plot showing the logarithmic fit of half-chain entanglement $S(t)$ for $p(q) = 2$ for a system size of $L = 4096$, the red line is given by the equation $S(t) = 0.5 + 0.333 \ln(t)$. (b) Similar plot but for $q = 4$, and the red line is given by the equation $S(t) = 0.01 + 0.67 \ln(t)$. (c) Same as (a) with $p = 10$. The red line indicates the fit $S(t) = -1.6047 + 1.66 \ln t$. (d) Same as (c) but with $q = 10$, and the red line denotes a fit $S(t) = -1.98 + 1.67 \ln t$. The inset in each figure shows the periodicity of the on-site potential used to simulate each plot.

charge is of value 1 for open boundary conditions, which is the configuration we study. For periodic potentials labeled by periodicity $p(q)$ the $c = p(q)$ is evident from Fig. 9. As can be seen from the insets of Figs. 9(a) and 9(b), the potential type $p(q)$ makes the lattice possess $Z_p(Z_q)$ symmetry. It seems $c = n$ where Z_n is the symmetry of the lattice.

We end this section by showing the limit in which our results correspond to the result of linear growth of EE from a defect site under inhomogeneous quench seen in Ref. [15] and bring in a new perspective. In our case, when $p \geq L/2$, we retrieve their results since then our system is identical to theirs except for the position of defect. An example of this can be seen in Fig. 10(b). In this plot the scattering center is positioned at $i = 3000$ in a lattice of size $L = 4096$. Thus, it is seen until the wave front reaches the scattering center, entanglement follows the $1/6 \ln t$ behavior for TI systems and then we see a linear rise for times longer than it. But in other cases discussed, contrary to their setup, we have

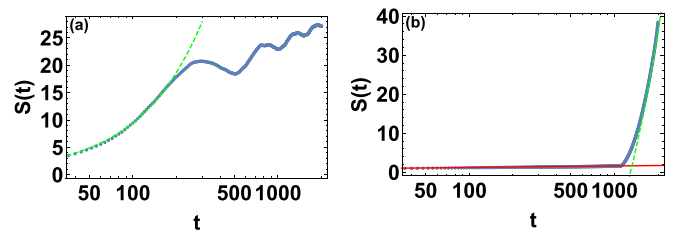


FIG. 10. (a) Plot showing the linear fit regime of half-chain entanglement $S(t)$ for $p = 32$ for a system size of $L = 4096$, and the red line is given by the equation $S(t) = 0.272 + 0.0917t$. (b) Plot showing the scenario for $p = 1500$ showing the two different fit regimes. The red line shows the fit to $0.467 + 0.167 \ln(t)$, and the green dashed line shows the fit to $-66 + 0.051t$.

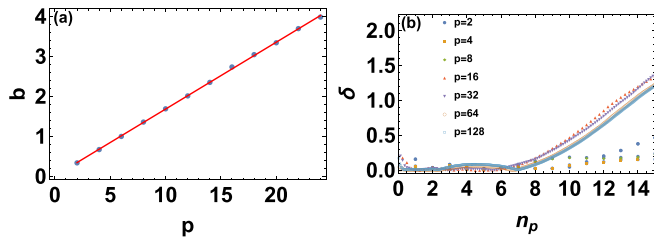


FIG. 11. (a) Plot of b , the coefficient of $\ln(t)$ in the fit of S vs p , the period of the potential, the red line is given by the equation $b = 0.004 + 0.167p$. (b) Plot of $\delta = |S - S^{\text{fit}}|/S$ vs $n_p = t/p$ showing when the values start deviating from linear fit. See the text for details.

multiple scattering centers, hence, the wave front undergoes multiple reflections, and the incident and reflected wave fronts interfere in a nontrivial manner to yield $\ln(t)$ rise in entanglement. Figure 11(b) gives an approximate timescale when our results show strong deviations from the linear increase in EE expected from a single defect. In this figure we plot the deviation relative deviation of entanglement entropy (S) with the linear fit at initial times ($t \leq 2p$), labeled S^{fit} and plot it against time (t) scaled by the periodicity (p) of the lattice considered. The rescaled time gives us an approximate idea of how many scattering sites the particle has crossed assuming ballistic propagation of particles. (A reasonable assumption for $\delta\mu = \mu = 0.1$ for the periodic potential. See the Supplemental Material [54]). It shows the linear rise is completely lost due to the interference of wave functions after the wave front crosses six to eight scattering sites. Figure 10(a) gives the dynamics for a $p = 32$ potential which shows how the fit changes from linear to logarithmic. Thus, one can put a bound of validity of the logarithmic fit in the last paragraph weakly at $p(q) < L/16$ from Fig. 11(b) as at periods lower than $L/16$ for the p -type potential, the wave front can cross more than eight scattering centers and shows the nonlinear rise in entanglement. Figure 12 shows how the eigenvalues ζ_l of the correlation matrix of the subsystem under consideration behave as the wave front travels through the lattice. It can be seen that if the timescales are small, and the wave front has not crossed more than one scattering center the newer nonzero eigenvalues entering into the correlation matrix are < 1 . The analysis of Ref. [15] points out that in such a case there will be a linear rise in entanglement due to a continued influx of $\zeta_l \neq 0, 1$ generated by the propagating wave front. But once $t > 2p$ this analysis is no longer valid as the wave front travels through more scattering centers, the scattered and incident wave fronts undergo interference, and there can be new ζ_l which are 0 or 1, thus, preventing the linear rise in entanglement entropy. A comparison of Figs. 12(b) and 12(d) reveals exactly this difference. This happens due to the coherent interference of scattered wave fronts which was absent in the setup considered by Ref. [15], however, a thorough understanding via analytical calculations is left for a future work. It is interesting to note that for disordered systems as Fig. 12(e) and 12(f) shows, the interference lacking the coherence of periodic systems, this effect is suppressed and, hence, the rise in entanglement entropy becomes faster and closer to single defect systems.

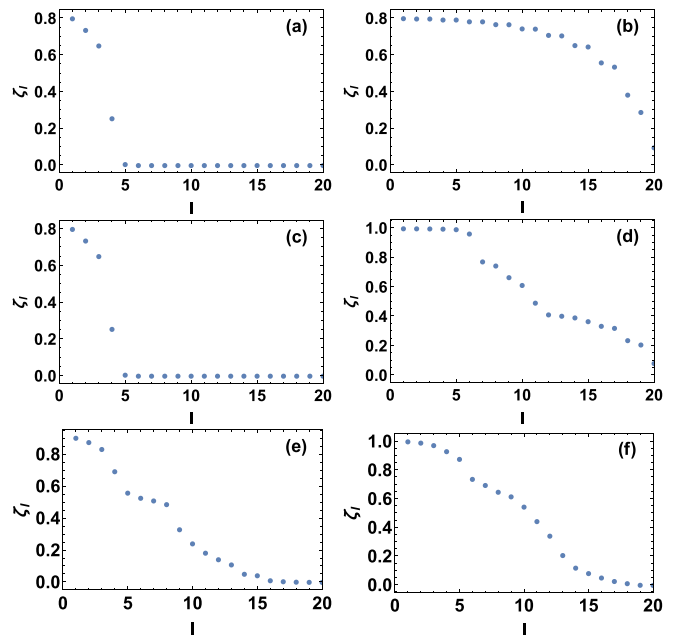


FIG. 12. (a) Plot of ζ_l , the eigenvalues of C_{ij} , correlation matrix of the subsystem $M = L/2 = 128$. Only the first 20 values are plotted. (a) In this system $\mu = \delta\mu = 0.25$ and $p = L/2$, i.e., only one scattering center is present at the subsystem environment interface. The eigenvalues are plotted at $t = 10$. (b) Same system as (a) except $t = 60$. (c) Here the eigenvalue at $t = 10$ is plotted for a system with $p = 16$ showing no quantitative difference with (a). (d) Same as (c) but at $t = 60$. Here we see a completely different result from (b) showing how an increasing number of eigenvalues are of value 1 and, thus, do not participate in entangling the subsystem and environment, thus, suppressing linear growth of entanglement for the single scattering center case. (e) Same parameters as (b) and (d) but in a system with random potential. (f) Same as (e) with the system having the Fibonacci potential and size $L = 377$. Note how in the last two cases the eigenvalue structure contains less eigenvalues closer to 1 than plot (d).

V. DISCUSSION

In this paper we have shown that the breaking of translation invariance in a one-dimensional free fermion system can result in an enhanced entanglement growth/information leakage compared to the translationally invariant case following an inhomogeneous quench. In disordered systems, this enhancement is observed in a subsystem of the size of the localization length. We identified backscattering of particles to the subsystem from its surrounding as the main mechanism behind the enhancement.

We also briefly touched upon the special case of breaking of TI by periodic potentials. There the coherent interference of the backscattered wave fronts produces certain peculiarities. For example, a larger spatial period p implies lesser number of backscatterers per unit length (locally closer to the TI case) but actually produces stronger enhancement in entanglement growth. We found for low periods there exists a $c/6 \ln t$ scaling of entanglement entropy very similar to the translationally invariant problem with $c = n$ where Z_n is the lattice symmetry. This is a rather interesting result in the sense these systems do not possess any conformal symmetry, and

we have similar behavior obtained as conformally invariant systems. We also recovered the linear rise regime at large periods and numerically analyzed when each regime sets in. We gave a weak bound on the value of period when one can expect to see the $\ln t$ scaling behavior. Then we discussed how the eigenvalues of the correlation matrix of the system change for lower periods compared to larger periods which changes the linear behavior to logarithmic. Interestingly, the pattern of new eigenvalues for the disordered lattice case follows the single scattering center scenario when one is within localization length. This points to a requirement of thorough analytical analysis of such systems as coherent scattering changes the physics completely. In principle, if one could analytically find closed form expression of the correlation functions in a periodic lattice from the single-particle eigenfunctions one can hope to analyze them to figure out this phenomenon. Since the one-particle eigenfunctions will pick up the symmetry of the lattice, there might be a possibility of extracting the coefficient of $\ln t$ finding how they combine to give the result. This is left for a future work.

The main result, namely, the enhancement of entanglement growth due to introduction of disorder betrays the nontrivial character of disordered quantum matter within the scale of localization length. This, to our knowledge, is a largely unexplored area. For weak disorder, this length scale can be considerable, and the understanding the physics might play a key role in designing quantum devices. An interesting open direction is to study the fate of this enhancement in the presence of weak interactions and external drive.

ACKNOWLEDGMENTS

R.G. thanks A. Sen for discussions and introducing him to problems with domain-wall initial states, K. Sengupta, S. Nandy, B. Mukherjee, and M. Sarkar for discussions and a CSIR SPM fellowship for financial support.

APPENDIX A: CALCULATION OF $\langle c_m^\dagger(t)c_n(t) \rangle$

Since this is a free fermion model, we can exploit the fact that all the information about the system is contained in the one-particle sector of the Hamiltonian. We can, thus, reduce the $2^N \times 2^N$ problem to the $N \times N$ problem in theory, but in practice, if we were to work in the Schrödinger picture we would have to still deal with $\binom{N}{m}$ eigenfunctions for a m -particle sector in a N -site model which are constructed as Slater determinants of the one-particle sector. But we are not interested in wave functions here, and, hence, we can switch to the Heisenberg picture, deal with $N \times N$ matrices, and find the required result. The entire procedure for this is as follows:

$$\mathcal{H} = Cc = c^\dagger R^\dagger RCR^\dagger Rc = b^\dagger Bb,$$

where c (c^\dagger) denotes a column (row) vector consisting of one-particle fermionic annihilation (creation) operators on each site. C denotes the matrix elements of the Hamiltonian in the one-particle occupation basis. $B = RCR^\dagger$ and $b^\dagger = c^\dagger R^\dagger$ or $b_i^\dagger = c_j^\dagger R_{ji}^\dagger = R_{ij}^* c_j^\dagger$ and $b_k = R_{kj} c_j$, B denotes the diagonalized matrix, and b denotes the diagonal basis. In this basis we know the Hamiltonian is $\mathcal{H} = -\sum_k E_k b_k^\dagger b_k$ ($E_k = B_{kk}$) and,

hence,

$$b_k(t) = b_k(0)e^{itE_k}, \quad b_k^\dagger(t) = b_k^\dagger(0)e^{-itE_k}. \quad (\text{A1})$$

Using these expressions we can write the time-dependent correlation matrix. Also we recall that $c = R^{-1}b = R^\dagger b$ or $c_i = R_{ij}^\dagger b_j = b_j R_{ji}^*$. Using this and remembering that for the systems considered in this paper the R matrices are all real,

$$\begin{aligned} \langle c_m^\dagger(t)c_n(t) \rangle &= \sum_{k,l} R_{km} R_{ln} \langle b_k^\dagger(t)b_l(t) \rangle \\ &= \sum_{k,l} R_{km} R_{ln} e^{-iE_k t} e^{iE_l t} \langle b_k^\dagger(0)b_l(0) \rangle \\ &= \sum_{k,l,i,j} R_{km} R_{ln} R_{ki} R_{lj} e^{i(E_k t - E_l t)} \langle c_i^\dagger(0)c_j(0) \rangle. \end{aligned} \quad (\text{A2})$$

Using the known initial conditions $\langle c_i^\dagger(0)c_j(0) \rangle$ we can calculate the evolution of the correlators to any instant of time.

APPENDIX B: THOULESS LOCALIZATION LENGTH

In this Appendix we give a brief idea about the calculation of Thouless localization length as defined by Ref. [46]. It gives the localization length of the single-particle eigenfunctions of a noninteracting Anderson localized system. For a system with a Hamiltonian as given by Eq. (1), the eigenstate equation is of the form

$$\mu_i a_i^\alpha - \frac{J}{2}(a_{i+1}^\alpha + a_{i-1}^\alpha) = E_\alpha a_i^\alpha, \quad (\text{B1})$$

where i runs from 1 to L and E^α is an eigenvalue of the system labeled by α , and a_i^α are the amplitudes of eigenstates. The Green's function of such a system can be written as

$$(E - \mu_i)G_{ij}(E) + \frac{J}{2}[G_{i+1,j}(E) + G_{i-1,j}(E)] = \delta_{ij}, \quad (\text{B2})$$

where $G_{ij} = (E\mathbf{I} - \mathbf{H}^{-1})$, \mathbf{H} being the Hamiltonian of the system. From this one can find G_{1N} as

$$G_{1N} = \left(\frac{J}{2}\right)^{N-1} \left/ \prod_{\alpha=1}^N (E - E_\alpha) \right. \quad (\text{B3})$$

Identifying G_{1N} has a pole of residue $a_1^\beta a_N^\beta$, and we can rewrite the equation as

$$n|a_1^\beta a_N^\beta| = (N-1) \ln \left| \frac{J}{2} \right| - \sum_{\alpha \neq \beta} \ln |E_\beta - E_\alpha|. \quad (\text{B4})$$

The key thing to note is now, for a localized eigenstate exponentially decays from its peak. Hence, if the peak is at site x one would expect $a_1 = \exp[-i\kappa(1-x)]$ and $a_N = \exp[-i\kappa(x-N)]$, where $\lambda = 1/\kappa$ is the localization length. Hence, in the limit of large L , one can define

$$\lambda = - \left[(N-1) \ln \left| \frac{J}{2} \right| - \sum_{\alpha \neq \beta} \ln |E_\beta - E_\alpha| \right]^{-1}. \quad (\text{B5})$$

Clearly for different E_β 's λ would be different. In our paper we consider $\lambda_l = \lambda_{\max}$, i.e., the largest Thouless localization length in the problem to provide an idea of the length scales.

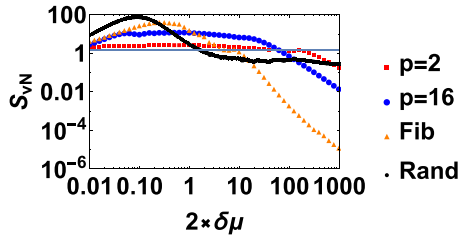


FIG. 13. Left: Plot showing Von Neumann entropy vs strength of inhomogeneity denoted by $\delta\mu$ at $t = 500$ for different representative cases. The subsystem is of length $M = L/2$, and the position of A is at $i = L/2 + 1$. The rest of the parameters are same as Fig 5(a).

APPENDIX C: A PECULIARITY OF THE ENTANGLEMENT AT HIGH $\delta\mu$

In Fig. 5(a) we showed the behavior EE with increasing $\delta\mu$ for different potentials when the subsystem AB is chosen from $i = L/2 + 21$ to $i = L$. As expected, for most of the cases the entanglement drops off as a power law with $\delta\mu$. It is also important to note different potentials follow a different power law which occurs due to the nature of scattering events encountered. It is to be expected correlated and uncorrelated scatterings result in different behaviors. Even in correlated

scattering the scattering from a periodic potential is different from a quasiperiodic one. The understanding of the various power laws observed is left for a future work.

Figure 13 shows the half-chain entanglement, and in this case A is taken at site $i = L/2 + 1$. Here as expected, when we are in the low disorder limit, the entanglement increases with disorder until a maximum after which it starts decreasing for all the cases of inhomogeneity. The random case shows the steepest ascent and descent compared to the other two cases. However at very high disorder entanglement still stays at a finite value. This peculiarity is due to the fact that for certain disorder realizations (which are significant in number) a very small particle density can be present in the $x > 0$ sector. This effectively ensures a finite number of wave fronts reaching the subsystem and carrying information even with a low particle density. This raises the entropy to a significant nonzero value even if the value is smaller compared to all other potentials. This event which causes such an anomaly in EE becomes exponentially smaller in number the further we move from $i = L/2$, hence, our choice of subsystem in the main text was such that these events do not interfere with our general analysis. However, in cases where we have considered a periodic potential or a Fibonacci potential, correlated scattering events show no such peculiarity.

- [1] V. Alba and F. Heidrich-Meisner, *Phys. Rev. B* **90**, 075144 (2014).
- [2] J. Mossel, G. Palacios, and J.-S. Caux, *J. Stat. Mech.: Theory Exp.* (2010) L09001.
- [3] T. Antal, Z. Rácz, A. Rákos, and G. M. Schütz, *Phys. Rev. E* **59**, 4912 (1999).
- [4] T. Antal, P. L. Krapivsky, and A. Rákos, *Phys. Rev. E* **78**, 061115 (2008).
- [5] V. Eisler and Z. Rácz, *Phys. Rev. Lett.* **110**, 060602 (2013).
- [6] J. Lancaster and A. Mitra, *Phys. Rev. E* **81**, 061134 (2010).
- [7] T. Sabetta and G. Misguich, *Phys. Rev. B* **88**, 245114 (2013).
- [8] M. Kormos, *SciPost Phys.* **3**, 020 (2017).
- [9] M. Kormos, C. P. Moca, and G. Zaránd, *Phys. Rev. E* **98**, 032105 (2018).
- [10] K. Klobas, M. Medenjak, and T. Prosen, *J. Stat. Mech.: Theory Exp.* (2018) 123202.
- [11] J. Viti, J.-M. Stéphan, J. Dubail, and M. Haque, *Europhys. Lett.* **115**, 40011 (2016).
- [12] I. Klich and L. Levitov, *Phys. Rev. Lett.* **102**, 100502 (2009).
- [13] H. F. Song, S. Rachel, C. Flindt, I. Klich, N. Laflorencie, and K. Le Hur, *Phys. Rev. B* **85**, 035409 (2012).
- [14] K. Bidzhiev and G. Misguich, *Phys. Rev. B* **96**, 195117 (2017).
- [15] V. Eisler and I. Peschel, *Europhys. Lett.* **99**, 20001 (2012).
- [16] E. Tonni, J. Rodríguez-Laguna, and G. Sierra, *J. Stat. Mech.: Theory Exp.* (2018) 043105.
- [17] T. Rakovszky, C. W. von Keyserlingk, and F. Pollmann, *Phys. Rev. B* **100**, 125139 (2019).
- [18] G. Refael and J. E. Moore, *Phys. Rev. Lett.* **93**, 260602 (2004).
- [19] G. Refael and J. E. Moore, *J. Phys. A: Math. Theor.* **42**, 504010 (2009).
- [20] N. Laflorencie, *Phys. Rev. B* **72**, 140408(R) (2005).
- [21] M. Fagotti, P. Calabrese, and J. E. Moore, *Phys. Rev. B* **83**, 045110 (2011).
- [22] J. Dubail, J.-M. Stéphan, and P. Calabrese, *SciPost Phys.* **3**, 019 (2017).
- [23] P. Ruggiero, V. Alba, and P. Calabrese, *Phys. Rev. B* **94**, 035152 (2016).
- [24] V. Eisler and D. Bauernfeind, *Phys. Rev. B* **96**, 174301 (2017).
- [25] H. Ueda and T. Nishino, *J. Phys. Soc. Jpn.* **78**, 014001 (2009).
- [26] G. Vitagliano, A. Riera, and J. I. Latorre, *New J. Phys.* **12**, 113049 (2010).
- [27] G. Ramírez, J. Rodríguez-Laguna, and G. Sierra, *J. Stat. Mech.: Theory Exp.* (2014) P10004.
- [28] G. Ramírez, J. Rodríguez-Laguna, and G. Sierra, *J. Stat. Mech.: Theory Exp.* (2015) P06002.
- [29] J. Rodríguez-Laguna, S. N. Santalla, G. Ramírez, and G. Sierra, *New J. Phys.* **18**, 073025 (2016).
- [30] J. Rodríguez-Laguna, J. Dubail, G. Ramírez, P. Calabrese, and G. Sierra, *J. Phys. A: Math. Theor.* **50**, 164001 (2017).
- [31] V. Eisler, F. Iglói, and I. Peschel, *J. Stat. Mech.: Theory Exp.* (2009) P02011.
- [32] P. W. Anderson, *Phys. Rev.* **109**, 1492 (1958).
- [33] D. Basko, I. Aleiner, and B. Altshuler, *Ann. Phys. (NY)* **321**, 1126 (2006).
- [34] J. H. Bardarson, F. Pollmann, and J. E. Moore, *Phys. Rev. Lett.* **109**, 017202 (2012).
- [35] M. Serbyn, Z. Papić, and D. A. Abanin, *Phys. Rev. Lett.* **110**, 260601 (2013).
- [36] P. Calabrese and J. Cardy, *J. Stat. Mech.: Theory Exp.* (2016) 064003.

- [37] W.-f. Chuan, *Fibonacci Q.* **30**, 68 (1992).
- [38] W.-f. Chuan, Subwords of the golden sequence and the fibonacci words, in *Applications of Fibonacci Numbers: Volume 6 Proceedings of "The Sixth International Research Conference on Fibonacci Numbers and Their Applications," Washington State University, Pullman, Washington, 1994*, edited by G. E. Bergum, A. N. Philippou, and A. F. Horadam (Springer, Dordrecht, 1996), pp. 73–84.
- [39] J. Q. You, Q. B. Yang, and J. R. Yan, *Phys. Rev. B* **41**, 7491 (1990).
- [40] Results and details for two more such lattices generated, respectively, from the Thue-Morse and Rudin-Shapiro sequences are relegated to the Supplemental Material.
- [41] J.-P. Allouche and J. Shallit, in *Sequences and their Applications*, edited by C. Ding, T. Hellesteth, and H. Niederreiter (Springer, London, 1999), pp. 1–16.
- [42] J.-P. Allouche and J. Shallit, *Automatic Sequences. Theory, Applications, Generalizations* (Cambridge University Press, Cambridge, U.K., 2003), pp. xvi + 571.
- [43] J.-P. Allouche and L. Maillard-Teyssier, *Theor. Comput. Sci.* **412**, 2268 (2011).
- [44] I. Peschel, *J. Phys. A* **36**, L205 (2003).
- [45] H. Casini and M. Huerta, *J. Phys. A: Math. Theor.* **42**, 504007 (2009).
- [46] D. J. Thouless, *J. Phys. C* **5**, 77 (1972).
- [47] M. Ljubotina, M. Žnidarič, and T. Prosen, *Nat. Commun.* **8**, 16117 (2017).
- [48] V. B. Bulchandani and C. Karrasch, *Phys. Rev. B* **99**, 121410(R) (2019).
- [49] See Supplemental Material at <http://link.aps.org/supplemental/10.1103/PhysRevB.103.024202> for details on speed of particle propagation in various systems.
- [50] P. Calabrese and J. Cardy, *J. Stat. Mech.: Theory Exp.* (2007) P10004.
- [51] F. Iglói, G. Roósz, and Y.-C. Lin, *New J. Phys.* **15**, 023036 (2013).
- [52] D. Gobert, C. Kollath, U. Schollwöck, and G. Schütz, *Phys. Rev. E* **71**, 036102 (2005).
- [53] V. Eisler and I. Peschel, *J. Stat. Mech.: Theory Exp.* (2007) P06005.
- [54] See Supplemental Material at <http://link.aps.org/supplemental/10.1103/PhysRevB.103.024202> for detailed analysis.
- [55] S.-A. Cheong and C. L. Henley, *Phys. Rev. B* **69**, 075111 (2004).
- [56] S.-A. Cheong and C. L. Henley, *Phys. Rev. B* **69**, 075112 (2004).
- [57] P. Calabrese and J. Cardy, *J. Stat. Mech.: Theory Exp.* (2005) P04010.
- [58] P. Calabrese and J. Cardy, *Phys. Rev. Lett.* **96**, 136801 (2006).
- [59] V. Alba, P. Calabrese, and E. Tonni, *J. Phys. A: Math. Theor.* **51**, 024001 (2017).
- [60] E. H. Lieb and D. W. Robinson, in *Statistical Mechanics: Selecta of Elliott H. Lieb*, edited by B. Nachtergaele, J. P. Solovej, and J. Yngvason (Springer, Berlin, Heidelberg, 2004), pp. 425–431.